Available online at www.sciencedirect.com
SCIENCE DIRECT®
Journal of Organometallic Chemistry 687 (2003) 337–345
Journal of Organometallic Chemistry
www.elsevier.com/locate/jorganchem

# The silicon effect on the regioselectivity of the Tsuji-Trost reaction. Experimental and theoretical approaches

Vicenç Branchadell [a], Marcial Moreno-Mañas [a,*], Roser Pleixats [a], Serge Thorimbert [b,*], Claude Commandeur [b], Cécile Boglio [b], Max Malacria [b,*,1]

[a] Department of Chemistry, Universitat Autònoma de Barcelona, Cerdanyola del Valles, 08193 Barcelona, Spain
[b] Université P. et M. Curie, Laboratoire de Chimie Organique, UMR 7611 CNRS, Tour 44-54, BP 229, 4, place Jussieu, F-75252 Paris Cedex 5, France

Received 28 May 2003; accepted 7 July 2003

Dedicated to Prof. Jean-Pierre Gênet on occasion of his 60th birthday

**Abstract**

Regioselectivity of the Tsuji-Trost reaction on allyl acetates and carbonates substituted with silyl groups at the olefinic moiety has been analyzed. Silicon atom in the central carbon atom increases the stability of the intermediate π-allylpalladium cation with respect to the isomeric π-allylpalladium cation featuring the silicon in a terminal carbon atom.


*Keywords:* Tsuji-Trost reaction; Regioselectivity; Silicon effect; Calculations

## 1. Introduction

The palladium-catalyzed allylation of nucleophiles (Tsuji-Trost reaction) is a useful synthetic method due to its broad scope, facile operation, and stereochemical outcome since many nucleophiles react with overall retention of configuration at the electrophile [1]. Attack of a palladium(0) species on the allyl derivative affords the cationic π-allylpalladium intermediate **1** (Scheme 1). This cation reacts at both terminal positions giving rise to isomers **2** and **3**. Very frequently the ratio **2/3** is dominated by steric factors, although electronic effects are also important [2]. Generally X is acetate or carbonate.

Silicon at the terminal carbon atoms in intermediate cations **1** ($R' = SiR_3$) play a curious role. Thus, attack by nucleophiles occurs at the remote position with respect to the silicon, even if R in cation **1** is more sterically demanding than $SiR_3$ (Scheme 1) [3]. This problem has been addressed by theoretical calculations [4].

Another different silicon effect has been found by some of us during the study of 2-silyl-2-butene-1,4-diol derivatives [5]. Thus, diacetate **4a** reacts chemo- and stereoselectively with carbon soft nucleophiles to afford **5a** as a 98/2 mixture of two stereoisomers, the indicated one predominating (Scheme 2). This introduces the question of the relative stability of ion pairs **6a** and **7a**. Indeed the formation of **5a** should occur exclusively via **6a**.

More striking is the reaction of acetate–carbonate **4b** with carbon nucleophiles to afford **5b** [5]. Acetate acts as leaving group in spite of the recognized better ability of carbonates as leaving groups in this type of chemistry [6]. The question now is if the stability of **6b** is higher enough to overcome the usual leaving group abilities. In summary, the real question is if a silicon atom in the central position of the cation has a more stabilizing effect than in a terminal position. This is reminiscent although not necessarily related to the stabilization of carbocations by silicon placed in the β position [7]. In this paper we present some more examples of this second type of silicon effect complemented with theoretical

* Corresponding authors.: Tel.: +34-93-581-1254; fax: +34-93-581-1265.
*E-mail addresses:* marcial.moreno@uab.es (M. Moreno-Mañas), malacria@ccr.jussieu.fr (M. Malacria).
[1] Tel.: +33-14-427-3585; fax: +33-14-427-7360.

0022-328X/03/$ - see front matter © 2003 Elsevier B.V. All rights reserved.
doi:10.1016/S0022-328X(03)00664-8

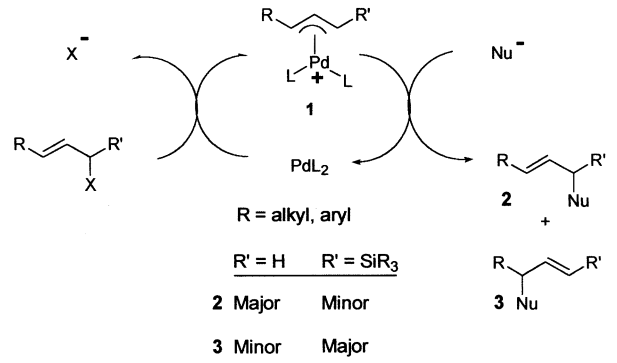


Scheme 1. General mechanistic and regiochemical features of the Tsuji-Trost reaction.

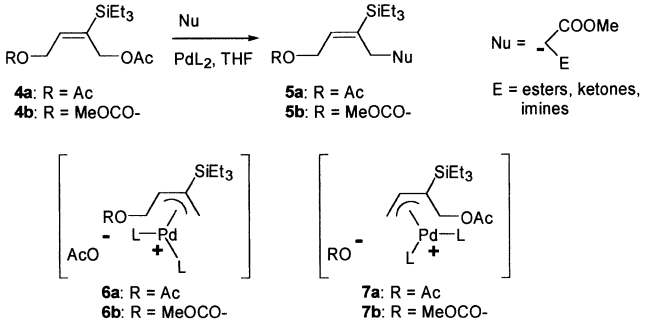


Scheme 2. Possible π-allylpalladium cations involved in the Tsuji-Trost reactions of compounds **4**.

calculations in order to gain a better understanding of the phenomenon.

## 2. Experimental

Compounds **4a** and **4b** (Scheme 3) were prepared from the commercially available 2-butyne-1,4-diol. Mono- or di-acetylation of the diol was followed by a stereoselective *syn* hydrosilylation of the triple bond using Speier's catalyst [8]. (*E*)-Silyl-substituted diacetate **4a** was isolated in nearly quantitative yield whereas the two regioisomers of the (*E*)-silyl-substituted acetate–alcohol were obtained in 69% yield as an 80/20 mixture [9]. After purification of the desired regioisomer by column chromatography through silica gel, reaction with methyl chloroformate gave the silylated acetate–carbonate **4b**. Submission of diacetate **4a** to usual palladium-catalyzed alkylation (dimethyl malonate or methyl acetoacetate sodium salt, $Pd(OAc)_2$, dppe) results in the completely chemoselective substitution of the acetate in the β position relative to the silicon group (Scheme 3). Compound **4b** reacted similarly with a slight erosion of the chemoselectivity. Thus, for **4b** ionization also took place mainly at the β position; however, some ionization of the carbonate was also observed. Reaction with dimethyl malonate gave in 85% yield (based on recovered starting material) an 80/20 mixture of **5b** and **9**. On the other hand reaction of **4b** with methyl acetoacetate gave a mixture of three compounds in 84% overall yield. Purification of the mixture over silica gel allowed the isolation of **5b′** in 30% yield as well as a 56/44 inseparable mixture of two furan-type compounds **8** and **10** in 54% yield. These are the result of a second palladium-catalyzed intramolecular alkylation. The allylsilane **8** derives from the expected compound **5b′** while the vinylsilane **10** comes from the alternative alkylation product **9′**.

Having established the reactivity of compounds **4a**, **b** with carbon nucleophiles, we extended our study to nitrogen nucleophiles. Reactions with benzylamine were unsuccessful in THF. Changing to *i*-PrOH proved to be favorable allowing the reaction to occur smoothly. Thus, product **11** derived from the substitution of the acetate in β position relative to silicon was obtained in low yield in addition to *N*-benzyl-3-(triethylsilyl)-2,5,dihydropyrrole, **12** (Scheme 4).

Then, we studied the reaction of *N*-tosylglycine methyl ester with diacetate **4a**, which gave the expected compound **13** in 50% yield with no trace of the product derived from the substitution of the γ acetate. In summary, the directing silicon effect seems to be independent of the nature of the nucleophile.

## 3. Theoretical calculations

In order to gain a better insight with respect to the experimental results, we have studied the formation of the model allylpalladium cations **16a** and **16b** from **14** and $Pd(PR_3)_2$ via cations **15** (Scheme 5) in a purely theoretical pathway, since the oxidative addition of Pd(0) to **14** is a one-step process involving simultaneous dissociation of acetate and addition of $PdL_2$. We have considered $PH_3$ and dppe as ligands. We will present the results obtained for $PH_3$ in the first place. To analyze the influence of the position of the TMS group we have also studied the model allylpalladium cations **18a** and **18b** (Scheme 6). Fig. 1 presents the optimized structures of the allylpalladium cations **16a**, **16b**, **18a**, and **18b**.

The formation of **16a** and **16b** from **14** and $Pd(PH_3)_2$ can be decomposed in two steps: loss of an acetate to generate allyl cations **15a** and **15b** and coordination of these cations to Pd (Scheme 5). Table 1 presents the reaction energies and Gibbs energies corresponding to these processes in gas phase, THF, and acetone. THF was the initial solvent tested for the transformations involving carbon nucleophiles (**4** into **5**) (Scheme 3) [5]. Moreover, better experimental results were obtained in isopropanol (vide supra) when working with nitrogen-based nucleophiles. Since isopropanol could not be introduced in our calculations, we selected acetone, very close to isopropanol in terms of polarity (dielectric

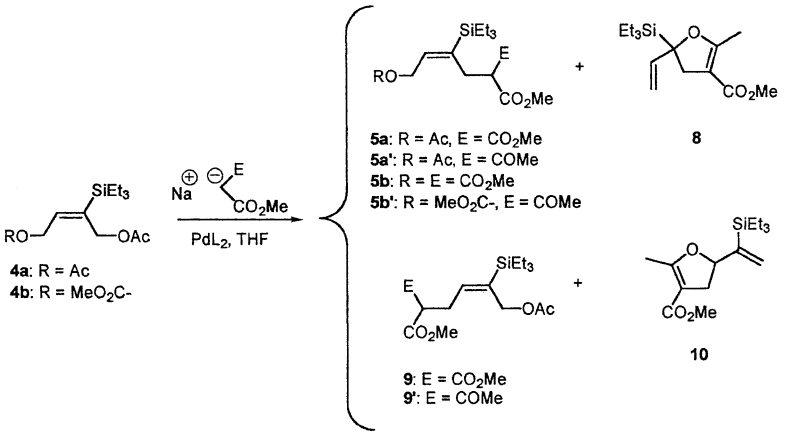


| Entry | 4. | E | 5 (%)[a] | 9 (%)[a] | 8 (%) + 10 (%)[a,b] | 5+8/9+10[c] | ref |
|---|---|---|---|---|---|---|---|
| 1 | 4a | $CO_2Me$ | 5a (95) | / | / | 100/0 | [5] |
| 2 | 4a | COMe | 5a' (71) | / | 8 (15) | 100/0 | d |
| 3 | 4b | $CO_2Me$ | 5b (64) | 9 (5) | / | 80/20 | d |
| 4 | 4b | COMe | 5b' (30) | / | 8 (30); 10 (24) | 70/30 | d |

(a) Isolated yield. (b) **10** was obtained as an inseparable mixture with **8**. (c) Based on $^1H$ NMR of the crude mixture. (d) This work.

Scheme 3. Reactions of sillyl-compounds **4** with carbon nucleophiles.

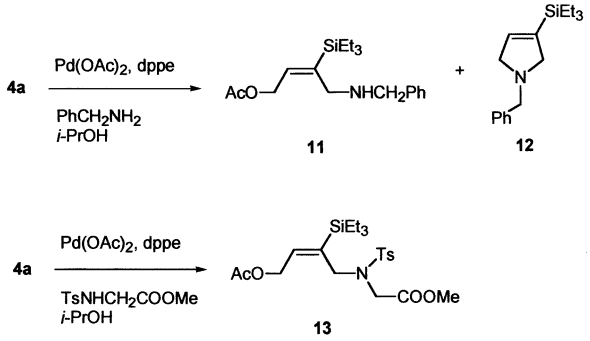


Scheme 4. Reactions of sillyl-compounds **4a** with nitrogen nucleophiles.

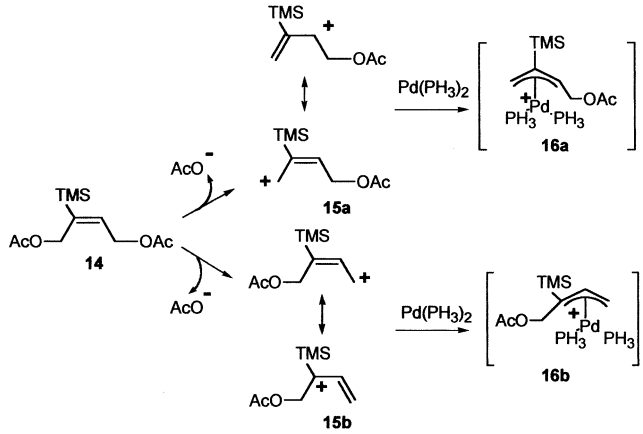


Scheme 5. Formal pathway for the formation of π-allylpalladium cations **16a**, **b**.

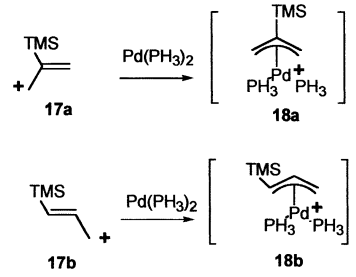


Scheme 6. π-Allylpalladium complexes **18a**, **b**.

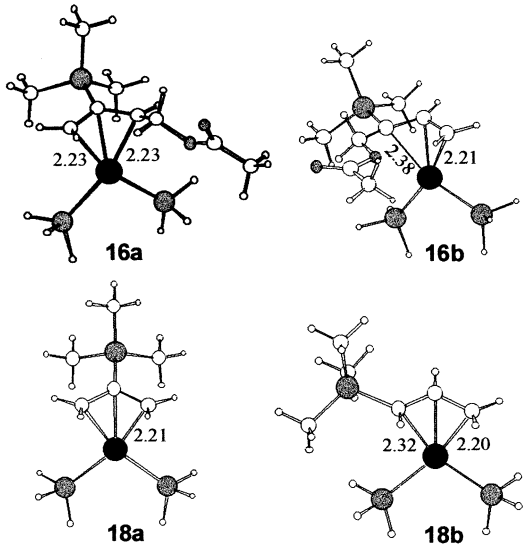


Fig. 1. Geometry of allylpalladium cations. Selected interatomic distances in angstrom.

Table 1
Energies and Gibbs energies [a] in the gas phase and in solution corresponding to the formation of allylpalladium cations [b]

| | 14 → 15a | 15a → 16a | 14 → 16a | 14 → 15b | 15b → 16b | 14 → 16b | 16a → 16b |
|---|---|---|---|---|---|---|---|
| $\Delta E$ | 167.7 | −59.7 | 108.0 | 163.8 | −51.5 | 112.3 | $\Delta\Delta E = 4.3$ |
| $\Delta G$ | 142.7 | −45.0 | 97.7 | 139.1 | −35.6 | 103.5 | $\Delta\Delta G = 5.8$ |
| $\Delta G_{THF}$ | 51.8 | −34.6 | 17.2 | 49.3 | −29.1 | 20.2 | $\Delta\Delta G_{THF} = 3.0$ |
| $\Delta G_{Acet.}$ | 43.0 | −37.4 | 5.6 | 40.8 | −28.8 | 12.0 | $\Delta\Delta G_{Acet.} = 6.4$ |

[a] In kcal mol$^{-1}$. Gibbs energies at 1 atm and 298.15 K computed with the B3LYP method.
[b] See Scheme 5.

constants: $\varepsilon_{isopropanol} = 19.92$; $\varepsilon_{acetone} = 20.56$) [10]. The dissociation step involves charge separation, so that it is very unfavorable in the gas phase. The inclusion of solvent effects stabilizes the reaction products, but the process is still endergonic. On the other hand, the coordination step is exothermic, but not enough to make the global process thermodynamically favorable.

Our treatment of solvent effects can only be considered as a first approximation, since solvent molecules have not been explicitly considered and the geometries have been kept the same as in the gas phase calculation. However, the results are expected to correctly describe the relative stabilities of the isomeric allylpalladium cations **16a** and **16b**. In summary, cation **16a** is more stable than **16b** as shown in the last column of Table 1.

Regarding the acetate dissociation step, Table 1 shows that the formation of **15b** is slightly favored with respect to the formation of **15a**. This is due to the different stabilities of the resulting cations. In both cases the C–C double bond and the positive charge are delocalized over the allyl moiety. In **15a** the positive charge can be placed at primary or secondary carbon atoms, whereas for **15b** the charge can be placed at a tertiary carbon. The structures of these cations are shown in Fig. 2.

Regarding the second step in the formation of the allylpalladium cations (Scheme 5), Table 1 shows that the coordination to $Pd(PH_3)_2$ is more favorable for **15a** than for **15b**.

Thus, the stabilities of the isomeric allylpalladium cations **16a** and **16b** are determined by the strength of the allyl–Pd bond. We have also studied the allyl coordination step for the model allyl cations **17a** and **17b** (Scheme 6) and the computed coordination energies are −71.1 and −61.5 kcal mol$^{-1}$, respectively. These results show that the presence of the TMS group at the allyl central carbon atom leads to a stronger Pd–allyl interaction.

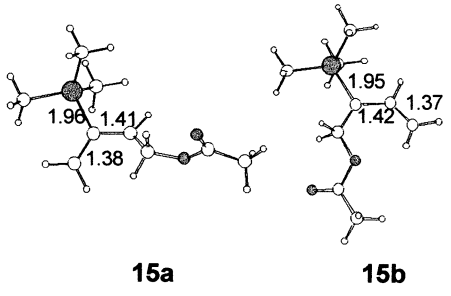


Fig. 2. Geometries of allyl cations. Selected interatomic distances in angstrom.

To understand the origin of this effect we have analyzed the different contributions to the binding energy. The energy of formation of an allylpalladium cation can be partitioned into two terms:

$$\Delta E = \Delta E_{prep} + \Delta E_{int}$$

The first term, $\Delta E_{prep}$, is the preparation energy, i.e. the energy necessary to distort the allyl cation and $Pd(PH_3)_2$ fragments from their equilibrium geometries to the geometries they have at the allylpalladium complex. The second term, $\Delta E_{int}$, is the interaction energy between both fragments. This term can be further partitioned in the following contributions:

$$\Delta E_{int} = \Delta E_{elstat} + \Delta E_{Pauli} + \Delta E_{orb}$$

$\Delta E_{elstat}$ represents the electrostatic interaction between the prepared fragments, each fragment having the electron density that would have in the absence of the other fragment. $\Delta E_{Pauli}$ is the Pauli repulsion term and arises from the ortho-normalization of the occupied fragment orbitals to obtain an antisymmetrized product and accounts for the closed shell repulsion between both fragments. Finally, $\Delta E_{orb}$ is the orbital interaction term that arises when the electron densities of the fragments are allowed to relax and takes into account the charge transfer between fragments and the polarization of both fragments. The results obtained in this analysis are

Table 2
Energy partition [a] for the coordination of allyl cations [b] to $Pd(PH_3)_2$

| | 15a → 16a | 15b → 16b | 17a → 18a | 17b → 18b |
|---|---|---|---|---|
| $\Delta E_{prep}$ | 30.5 | 29.1 | 25.7 | 27.0 |
| $\Delta E_{Pauli}$ | 208.7 | 190.7 | 197.0 | 189.0 |
| $\Delta E_{elstat}$ | −149.4 | −135.9 | −141.8 | −134.2 |
| $\Delta E_{orb}$ | −142.8 | −131.0 | −147.1 | −138.9 |
| $\Delta E$ | −53.0 | −47.1 | −66.2 | −57.1 |

[a] Computed with the BLYP method. In kcal mol$^{-1}$. See text for definitions.
[b] See Schemes 5 and 6.

Table 3
Orbital energies [a] of π orbitals of allyl cations

| | $CH_2CHCH_2^+$ | 15a | 15b | 17a | 17b |
|---|---|---|---|---|---|
| π | −0.5735 | −0.4914 | −0.4934 | −0.5407 | −0.5223 |
| nπ | −0.3851 | −0.3155 | −0.3094 | −0.3512 | −0.3357 |
| π* | −0.2164 | −0.1773 | −0.1547 | −0.1925 | −0.1746 |

See Schemes 5 and 6.
[a] In atomic unit.

summarized in Table 2. The complexation energies show the same trends as the values presented in Table 1, which where obtained at a different level of calculation.

The result of the energy partition shows that the preparation energy term has similar values for the formation of the two isomers. The formation of the allylpalladium cations involves repulsive and attractive interactions between the fragments. The strength of these interactions increases as both fragments approach one to another. The final geometry corresponds to a situation in which the attractive interactions overcompensate the repulsive ones. Fig. 1 shows that for **16a** and **18a** the distances between palladium and both allyl terminal carbon atoms have the same value. On the other hand, for **16b** and **18b** we observe differences of 0.17 and 0.12 Å, respectively. These differences may have a steric or an electronic origin. The presence of the TMS group induces steric repulsion that may be reduced through a lengthening of the corresponding Pd–C bond with respect to the values obtained for **16a** and **18a**. Electronic effects can be related to the shape of the empty nπ orbital of the allyl cations. For **17a** the contribution of both allyl terminal carbon atoms to this orbital is the same, so that the resulting complex **18a** is symmetric. For the non-symmetrical allyl cation **17b** the nπ orbital is slightly polarized towards the carbon bearing the TMS group.[2]

So, electron donation from the HOMO of $Pd(PH_3)_2$ to the LUMO of the allyl cation would favor a short Pd–C(TMS) distance in **18b**. The values of the Pd–C distances obtained for this complex (see Fig. 1) show that steric effects are predominant.

As a result of the sterically-induced changes in geometry, the Pauli, electrostatic, and orbital interaction terms are stronger for **16a** and **18a** than for **16b** and **18b**, respectively.

The relative values of the orbital interaction term can be related to the electron acceptor ability of the allyl cations. Table 3 presents the energies of the allyl π orbitals of **15a**, **15b**, **17a**, and **17b**. We have also included the parent allyl cation for comparison.

[2] The sum of the squares of the coefficients corresponding to C 2p orbitals for the two terminal carbon atoms is 0.360 and 0.338, respectively.

The presence of the TMS group increases the energies of the empty nπ and π* orbitals, so that the substituted allyl cations become worse electron acceptors than the parent cation. The effect of TMS is more notorious when it is bonded at one of the allyl terminal carbon atoms, so that **17b** should be a worse electron acceptor than **17a**. These electronic effects would contribute to the larger stability of **16a** with respect to **16b**.

We have studied the attack of ammonia, as a model nucleophile, to the less substituted allyl terminal carbon atom of the allylpalladium cations and we have located the transition states. The structures of these transition states are presented in Fig. 3 and the corresponding potential energy barriers and Gibbs activation energies are shown in Table 4. We can observe that the solvent effect on the nucleophilic attack is small.

The reaction with **16b** involves a lower energy barrier than the reaction with **16a**. Similar results are obtained for **18a** and **18b**. These results suggest that allylpalladium cations with a TMS group at one of the allyl terminal carbon atoms are better electrophiles than cations in which the TMS group is at the central carbon atom. The nucleophilic attack mainly involves the interaction between the lone pair of the nucleophile and the LUMO of the allylpalladium cation. This orbital is the antibonding combination of the nπ orbital of the allyl moiety and one of the 4d orbitals of Pd. Table 5 shows that the energy of the LUMO is lower when the TMS group is at the terminal carbon (**16b** and **18b**) than when it is at the central carbon (**16a** and **18a**).

Allylpalladium cations with a TMS group at one of the allyl terminal carbon atoms are more reactive than

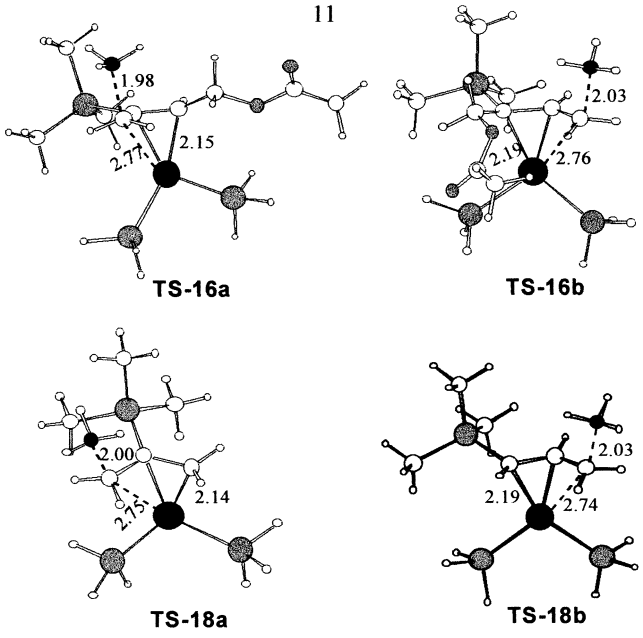


Fig. 3. Structures of the transition states corresponding to the nucleophilic attack of ammonia to allylpalladium cations. Selected interatomic distances in angstrom.

Table 4
Potential energy barriers and Gibbs activation energies [a] in the gas phase and in solution for the attack of ammonia to the less substituted terminal allyl carbon atom of allylpalladium cations

| | 16a | 16b | 18a | 18b |
|---|---|---|---|---|
| $\Delta E^{\ddagger}$ | 3.7 | 0.6 | 3.3 | 2.4 |
| $\Delta G^{\ddagger}$ | 17.5 | 13.2 | 14.5 | 14.1 |
| $\Delta G^{\ddagger}_{THF}$ | 18.6 | 15.0 | 15.9 | 15.3 |
| $\Delta G^{\ddagger}_{Acetone}$ | 18.5 | 15.2 | 15.8 | 15.1 |

See Fig. 3.
[a] In kcal mol$^{-1}$. Gibbs energies at 1 atm and 298.15 K computed with the B3LYP method.

Table 5
Energy [a] of the LUMO for allylpalladium cations

| | E |
|---|---|
| **16a** | −0.2041 |
| **16b** | −0.2106 |
| **18a** | −0.2057 |
| **18b** | −0.2128 |

See Schemes 5 and 6.
[a] In atomic unit.

cations with a central TMS ($\Delta\Delta G^{\ddagger} = 3.3$ kcal mol$^{-1}$ in acetone, for **16a** and **16b** Table 4). However, the difference of reactivities is smaller than the difference in the Gibbs energies of formation of the allylpalladium cations ($\Delta\Delta G = 6.4$ kcal mol$^{-1}$ in acetone, Table 1). As a result, the observed regioselectivity is governed by the stabilities of the isomeric allylpalladium cations.

Up to now we have considered $PH_3$ as a ligand for Pd. We should verify that the conclusions are still valid for a more realistic model. For this reason we have studied the formation of analogs of **16a** and **16b** and their reactions with ammonia using dppe as phosphine ligand. For the allylpalladium cations **19a** and **19b**, we have optimized the geometries without any restriction. On the other hand, for the transition states we have kept frozen the distance corresponding to the forming bond in the nucleophilic attack at the values obtained for the systems with $PH_3$ and we have optimized the rest of the geometry. The structures obtained for the allylpalladium cations and for the model transition states are shown in Fig. 4. Table 6 presents the values of the energy of formation of these cations from the coordination of **15a** and **15b** to Pd(dppe) and the potential energy barriers corresponding to the nucleophilic attack by ammonia.

The comparison of these coordination energies with those corresponding to the $PH_3$ complexes **16a** and **16b** (Table 1) shows that the interaction is notably stronger when the phosphine ligand is dppe. It should be taken into account that the presence of the Ph groups in dppe involves steric requirements that were absent for $PH_3$.

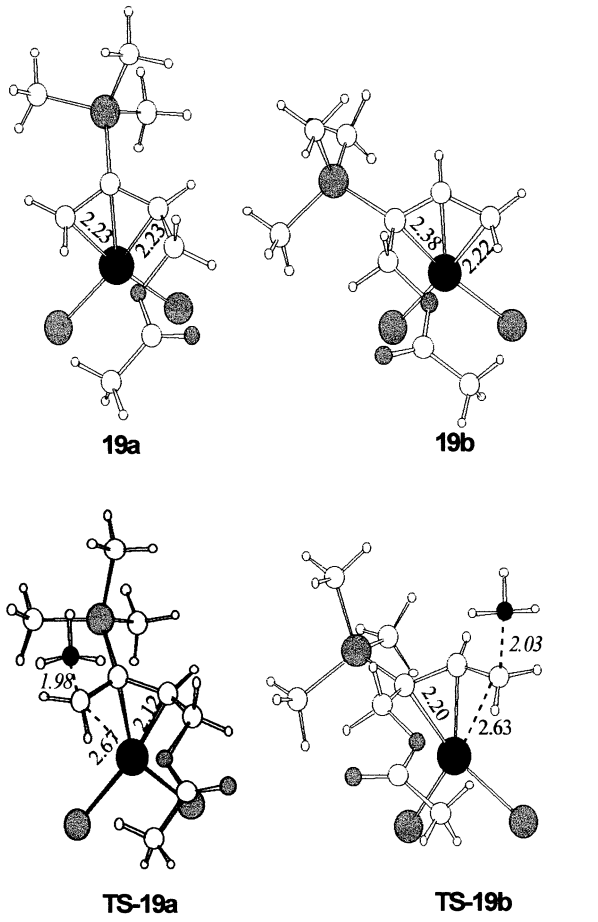


Fig. 4. Structures of allylpalladium cations and of transition states corresponding to nucleophilic attack by ammonia. The substituents of the dppe ligand have been omitted for clarity. Selected interatomic distances in angstrom.

Table 6
Energy of coordination of allyl cations to Pd(dppe) and potential energy barrier [a] for the attack of ammonia to the less substituted allyl terminal carbon atom of the allylpalladium cations

| | 19a | 19b |
|---|---|---|
| $\Delta E$ | −83.0 | −76.0 |
| $\Delta E^{\ddagger}$ | 13.3 | 12.5 |

See Fig. 4.
[a] In kcal mol$^{-1}$, computed with the B3LYP method.

On the other hand, dppe is a better electron donor than $PH_3$ and the energies of the HOMO of the $PdL_2$ fragments are −0.1876 a.u. for $PH_3$ and −0.1521 a.u. for dppe. The fact that the coordination energy becomes more negative indicates that these electronic effects overcompensate the steric repulsions. As a result, the energies of formation of **19a** and **19b** from **14** and Pd(dppe) are 84.7 and 87.8 kcal mol$^{-1}$, respectively. That is, 23.3 and 24.5 kcal mol$^{-1}$ lower than the values computed for **16a** and **16b**, respectively. If we assume that a similar lowering can be applied to the $\Delta G$

computed for **16a** and **16b**, the processes would become exergonic in solution.

The attack of ammonia becomes less favorable. Fig. 4 shows that for the model transition states **TS-19a** and **TS-19b** the distances between Pd and the allyl terminal carbon atoms are smaller than for **TS-16a** and **TS-16b** (see Fig. 2). As we have already seen, the Pd–allyl bond is stronger for the dppe complexes than for the $PH_3$ ones. The nucleophilic attack involves a partial cleavage of this bond so that there is a correlation between the potential energy barrier and the strength of the bond. The computed potential energy barriers also show that the attack to **19b** is more favorable than to **19a** and that the difference of barriers is smaller than the difference of stabilities of both isomeric allylpalladium cations.

## 4. Conclusions

Calculations show that the presence of silicon in the central carbon atom of π-allylpalladium cations causes stronger Pd–allyl interaction, therefore justifying that these cations are more stable than their isomers possessing silicon at the terminal carbon atoms. These differences in stability overcome the intrinsic higher reactivity of π-allylpalladium cations featuring silicon at the terminal positions. These results are in complete agreement with the experimentally found regioselectivity of Tsuji-Trost reactions of carbon and nitrogen nucleophiles on these systems.

## 5. Experimental

### 5.1. General remarks

All reactions requiring anhydrous conditions were performed under a positive nitrogen or argon atmosphere using oven-dried glassware. All solvents were purified and distilled according to standard methods. Final product solutions were dried over $MgSO_4$ or $Na_2SO_4$, filtered, and evaporated under reduced pressure on a rotary evaporator. Thin layer chromatography was performed on silica gel 60 $F_{254}$. Chromatographic purifications were conducted using 40–63 μm or 15–40 μm silica gel. All compounds were isolated as oils unless otherwise specified. $^1$H-NMR ($^{13}$C-NMR) spectra were recorded at 200 (50) MHz and 400 (100) MHz. Chemical shifts are given in parts per million, referenced to the residual proton resonances of the solvents (7.25/77.16 ppm for $CDCl_3$). Coupling constants ($J$) are given in hertz (Hz). The letters m, s, d, t, q, mean respectively multiplet, singlet, doublet, triplet, quartet. The letters br mean the signal is broad. Infrared spectra were recorded on a Bruker Tensor 27 spectrophotometer by attenuated total reflection. All IR data are reported in wavenumber ($cm^{-1}$).

### 5.2. Alkylation of *4b* with carbon nucleophiles

#### 5.2.1. (*E*)-2-(4-Methoxycarbonyloxy-2-triethylsilanyl-but-2-enyl)-malonic acid dimethyl ester (*E*)-*5b*

At 0 °C, under argon, to a suspension of sodium hydride 60% in mineral oil (40 mg, 1 mmol), in THF (3 ml) was added dropwise dimethyl malonate (0.12 ml, 1 mmol) and the reaction mixture was warmed to room temperature (r.t.) for 30 min. In a separate flask, $Pd(OAc)_2$ (11 mg, 5 mol%) was dissolved in THF (1 ml), diphenylphosphinoethane (40 mg, 8 mol%) was added and the solution was stirred for 30 min. Then, acetate–carbonate **4b** (302 mg, 1 mmol) was added and the resulting mixture was dropwise transferred through a cannula to the malonate anion. After 4 h, the solution was diluted with $Et_2O$ and washed with a saturated solution of ammonium chloride. The aqueous phase was extracted with $Et_2O$ and the combined organic layers were washed with brine, dried over $MgSO_4$ and filtered. The solvent was evaporated under reduced pressure giving a mixture of **5b** and **9**. Purification by flash chromatography on a silica gel column affords **5b** (247 mg, 64%, e/z = 90/10), 58 mg of starting material **4b** (19%), and product **9** (19 mg, 5%, e/z = 70/30) all as colourless oils.

**5b**: $^1$H-NMR ($CDCl_3$, 400 MHz) $\delta$ 5.86 (t, 1H, $J$ = 6.0 Hz); 4.78 (d, 2H, $J$ = 6.0 Hz); 3.77 (s, 3H); 3.70 (s, 6H); 3.42 (t, 1H, $J$ = 8 Hz); 2.77 (d, 2H, $J$ = 8 Hz); 0.89 (t, 9H, $J$ = 8.0 Hz); 0.60 (q, 6H, $J$ = 8.0 Hz); $^{13}$C-NMR ($CDCl_3$, 100 MHz) $\delta$ 170.8: (C); 169.2: (C); 138.5: (CH); 138.0: (C); 61.3: ($CH_2$); 52.6: ($CH_3$); 51.4: (CH); 29.6: ($CH_2$); 21.0: ($CH_3$); 7.2: ($CH_3$); 3.1: ($CH_2$); IR: 2956; 2876; 1734; 1437; 1264; 1149; 1025; 719. Anal. Calc. for $C_{17}H_{30}O_7Si$: C, 54.52; H, 8.07%. Found: C, 54.42; H, 8.25%.

#### 5.2.2. (*E*)-2-Acetyl-6-methoxycarbonyloxy-4-triethylsilanyl-hex-4-enoic acid methyl ester (*E*)-*5b′*

At 0 °C, under argon, to a suspension of sodium hydride 60% in mineral oil (21 mg, 0.52 mmol, 1.05 equivalent), in THF (1.5 ml) was added dropwise methyl acetoacetate (0.06 ml, 0.55 mmol, 1.1 equivalent) and the reaction mixture was warmed to r.t. for 30 min. In a separate flask, $Pd(OAc)_2$ (5.6 mg, 5 mol%) was dissolved in THF (0.5 ml), diphenylphosphinoethane (20 mg, 8 mol%) was added and the solution was stirred 30 min. Then, acetate–carbonate **4b** (151 mg, 0.5 mmol) was added and the resulting mixture was dropwise transferred through a cannula to the nucleophile. After 4 h, the solution was diluted with $Et_2O$ and washed with a saturated solution of ammonium chloride. The aqueous phase was extracted with $Et_2O$ and the combined organic layers were washed with brine, dried over

$MgSO_4$ and filtered. The solvent was evaporated under reduced pressure and the product was purified by flash chromatography on a silica gel column to afford **5b′** (56 mg, 30%, e/z = 90/10) as a colourless oil. The furan derivatives **8** and **10** were isolated as an inseparable 56/44 mixture (77 mg, 54%).

**5b′**: $^1$H-NMR ($CDCl_3$, 400 MHz) $\delta$ 5.83 (t, 1H, $J$ = 6.1 Hz); 4.79 (dd, part of ABX system, 1H, $J$ = 13.9 and 6.1 Hz); 4.72 (dd, part of ABX system, 1H, $J$ = 13.9 and 6.1 Hz); 3.74 (s, 3H); 3.68 (s, 3H); 3.47 (t, 1H, $J$ = 8.8 Hz); 2.73 (dd, part of ABX system, 1H, $J$ = 13.9 and 8.8 Hz); 2.60 (dd, part of ABX system, 1H, $J$ = 13.9 and 6.1 Hz); 2.19 (s, 3H); 0.87 (t, 9H, $J$ = 7.8 Hz); 0.58 (q, 6H, $J$ = 7.8 Hz); $^{13}$C-NMR ($CDCl_3$, 100 MHz) $\delta$ 201.9: (C); 169.8: (C); 155.7: (C); 139.3: (C); 137.5: (CH); 64.7: ($CH_2$); 59.0: ($CH_3$); 54.8: ($CH_3$); 52.6: (CH); 29.8: ($CH_3$); 29.4: ($CH_2$); 7.3: ($CH_3$); 3.2: ($CH_2$); IR: 2954; 2876; 1746; 1719; 1442; 1260; 1003; 949; 719. Anal. Calc. for $C_{17}H_{30}O_6Si$: C, 56.95; H, 8.43%. Found: C, 57.10; H, 8.60%.

### 5.2.3. 2-Methyl-5-triethylsilanyl-5-vinyl-4,5-dihydrofuran-3-carboxylic acid methyl ester **8**

$^1$H-NMR ($CDCl_3$, 400 MHz) $\delta$ 5.77 (dd, 1H, $J$ = 16.9 and 10.8 Hz); 5.03 (dd, 1H, $J$ = 17.2 and 1.3 Hz); 4.93 (dd, 1H, $J$ = 10.8 and 1.3 Hz); 3.66 (s, 3H); 3.00 (dd, part of ABX system, 1H, $J$ = 13.9 and 1.3 Hz); 2.73 (dd, part of ABX system, 1H, $J$ = 13.6 and 1.3 Hz); 2.17 (s, 3H); 0.94 (t, 9H, $J$ = 7.8 Hz); 0.60 (q, 6H, $J$ = 7.8 Hz); $^{13}$C-NMR ($CDCl_3$, 100 MHz) $\delta$ 168.4: (C); 166.9: (C); 141.7: (CH); 110.0: ($CH_2$); 100.6: (C); 86.1: (C); 50.9: ($CH_3$); 38.2: ($CH_2$); 14.2: ($CH_3$); 7.5: ($CH_3$); 1.4: ($CH_2$). Anal. Calc. for $C_{15}H_{26}O_3Si$: C, 63.78; H, 9.28%. Found: C, 63.83; H, 9.30%.

### 5.2.4. 2-Methyl-5-(1-triethylsilanyl-vinyl)-4,5-dihydrofuran-3-carboxylic acid methyl ester **10**

$^1$H-NMR ($CDCl_3$, 400 MHz) $\delta$ 5.79 (d, 1H, $J$ = 1.5 Hz); 5.38 (d, 1H, $J$ = 1.5 Hz); 5.13 (dd, 1H, $J$ = 10.6 and 9.3 Hz); 3.65 (s, 3H); 3.01 (ddd, part of $ABX_2$ system, 1H, $J$ = 13.9; 10.6 and 1.5 Hz); 2.57 (ddd, part of $ABX_2$ system, 1H, $J$ = 13.9; 9.3 and 1.5 Hz); 2.18 (s, 3H); 0.90 (t, 9H, $J$ = 7.8 Hz); 0.60 (q, 6H, $J$ = 7.8 Hz); $^{13}$C-NMR ($CDCl_3$, 100 MHz) $\delta$ 168.2: (C); 166.7: (C); 148.3: (C); 125.0: ($CH_2$); 101.3: (C); 85.5: (CH); 50.8: ($CH_3$); 36.6: ($CH_2$); 14.0: ($CH_3$); 7.3: ($CH_3$); 3.2: ($CH_2$); IR: 2952; 2876; 1706; 1649; 1222; 1086; 722.

## 5.3. Alkylation of diacetate **4a** with nitrogen-based nucleophiles

### 5.3.1. (E)-N-[(4-Acetoxy-2-triethylsilanyl-but-2-enyl)-N-(4-toluene-sulfonyl)]aminoacetic acid methyl ester (E)-**13**

At r.t., under argon, $Pd(OAc)_2$ (11 mg, 0.05 mmol, 5%) and diphenylphosphinoethane (60 mg, 0.15 mmol, 15%) were dissolved in *i*-PrOH (1.5 ml) and the solution was warmed at 50 °C during 30 min. A solution of diacetate **4a** (286 mg, 1 mmol) in *i*-PrOH (0.5 ml) was transferred through a cannula. Then a mixture of *N*-tosyl-glycine methyl ester (486 mg, 2 mmol, two equivalents) and $Et_3N$ (0.28 ml, 2 mmol, two equivalents) was added and the reaction mixture was warmed to 50 °C. After 4 h, the solution was diluted with $CH_2Cl_2$ and washed with a saturated solution of ammonium chloride. The aqueous phase was extracted with $CH_2Cl_2$ and the combined organic layers were washed with brine, dried over $MgSO_4$ and filtered. The solvent was evaporated under reduced pressure and the product was purified by flash chromatography on a silica gel column to afford **13** (235 mg, 50%, e/z = 80/20) as a colourless oil. $^1$H-NMR ($CDCl_3$, 400 MHz) $\delta$ 7.70 (d, 2H, $J$ = 8.5 Hz); 7.32 (d, 2H, $J$ = 8.5 Hz); 6.05 (t, 1H, $J$ = 6.2 Hz); 4.62 (d, 2H, $J$ = 6.2 Hz); 3.98 (s, 2H); 3.48 (s, 2H); 3.18 (s, 3H); 2.46 (s, 3H); 2.06 (s, 3H); 0.93 (t, 9H, $J$ = 8.2 Hz); 0.64 (q, 6H, $J$ = 8.2 Hz); $^{13}$C-NMR ($CDCl_3$, 100 MHz) $\delta$ 170.7: (C); 169.3: (C); 143.6: (C); 142.1: (CH); 136.3: (2C); 129.5: (CH); 127.6: (CH); 60.9: ($CH_2$); 51.9: ($CH_3$); 45.7: ($CH_2$); 45.6: ($CH_2$); 21.7: ($CH_3$); 20.9: ($CH_3$); 7.4: ($CH_3$); 2.6: ($CH_2$); IR: 2952; 2875; 1740; 1437; 1158; 718. Anal. Calc. for $C_{22}H_{35}O_6NSSi$: C, 56.26; H, 7.51; N, 2.98%. Found: C, 56.51; H, 7.70; N, 2.67%.

### 5.3.1.1. 1-Benzyl-3-triethylsilanyl-2,5-dihydro-1H-pyrrole **12**.

Compound **12** was prepared following the same procedure as for compound **13** from diacetate **4a** and benzylamine; $^1$H-NMR ($CDCl_3$, 400 MHz) $\delta$ 7.27 (m, 5H); 5.92 (s, 1H); 3.73 (s, 2H); 3.45 (s, 4H); 0.86 (t, 9H, $J$ = 7.8 Hz); 0.53 (q, 6H, $J$ = 7.8 Hz); $^{13}$C-NMR ($CDCl_3$, 100 MHz) $\delta$ 139.8: (C); 139.1: (C); 137.8: (CH); 128.6: (CH); 128.2: (CH); 126.8: (CH); 63.8: ($CH_2$); 61.4: ($CH_2$); 60.4: ($CH_2$); 7.4: ($CH_3$); 3.0: ($CH_2$).

## 5.4. Computational methods

All the calculations have been done using density functional (DFT) methods. The molecular geometries have been fully optimized using the hybrid Becke [11] functional for exchange and the correlation functional of Lee et al. [12] (B3LYP) implemented in the GAUSSIAN-98 program [13]. In these calculations we have used the effective core potentials of Hay and Wadt for Pd, P and Si [14]. For the remaining atoms, we have used the D95 basis set [14,15]. This basis set has been supplemented with a set of *d* polarization functions for C, N, Si, and P and a set of diffuse *d* functions of exponent 0.0628 for Pd. Harmonic vibrational frequencies have been calculated for all structures to verify that they are energy minimum (all frequencies are real) or transition states (only one imaginary frequency). For the C and H atoms of the dppe ligand we have used the Slater type

orbital (STO)-3G basis set [16]. Solvent effects have been taken into account using the conductor-like screening model [17] implemented in the GAUSSIAN-98 program. Two different solvents have been considered: THF ($\varepsilon = 7.6$) and acetone ($\varepsilon = 20.7$). In the calculation of the acetate elimination step in solution, the basis set has been augmented with diffuse *s* and *p* functions for C and O.

Single point calculations on the B3LYP optimized geometries have been done to analyze the Pd–allyl bond using the extended transition state method of Ziegler and Rauk [18] implemented in the ADF program [19]. In these calculations we have used the Becke's exchange functional [20] along with the Lee et al. [12] correlation functional (BLYP) and an uncontracted STO basis set. The inner electrons have been treated by the frozen-core approximation [21]. For the valence space, the used basis set is triple-ζ for Pd and double-ζ for the remaining atoms. A set of *d* polarization functions has been added for C, N, Si, and P.

## Acknowledgements

Financial support from MCyT of Spain (Project BQU2002-04002-C02) and Generalitat de Catalunya (Project SGR 2001-00181) is acknowledged. Computational time from CESCA is gratefully acknowledged. We thank the CNRS for financial support and the MNERT for a grant to C.C. This collaboration has been carried under the auspices of the COST program (COST D12/0011/98 and D24/0013-02 working groups).

## References

[1] E. Negishi (Ed.), Handbook of Organopalladium Chemistry for Organic Chemistry (Chapter V), Wiley–Interscience, New York, 2002 (Chapter V).
[2] (a) M. Prat, J. Ribas, M. Moreno-Mañas, Tetrahedron 48 (1992) 1695;
(b) M. Moreno-Mañas, F. Pajuelo, T. Parella, R. Pleixats, Organometallics 16 (1997) 205;
(c) V. Branchadell, M. Moreno-Mañas, F. Pajuelo, R. Pleixats, Organometallics 18 (1999) 4934;
(d) F. Delbecq, C. Lepouge, Organometallics 19 (2000) 2716.
[3] For the first case described as far as we know see: T. Hirao, J. Enda, Y. Ohshiro, T. Agawa, Tetrahedron Lett. 22 (1981) 3079. See also references in [4].
[4] V. Branchadell, M. Moreno-Mañas, R. Pleixats, Organometallics 21 (2002) 2407 (and references cited therein).
[5] (a) S. Thorimbert, M. Malacria, Tetrahedron Lett. 37 (1996) 8483;
(b) C. Commandeur, S. Thorimbert, M. Malacria, J. Org. Chem. 68 (2002) 5588.
[6] M. Moreno-Mañas, R. Pleixats, in Ref. [1], pp. 1707–1767 (Chapter V.2.1.3).
[7] J.S. Panek, in: B.M. Trost, I. Fleming (Eds.), Comprehensive Organic Synthesis, vol. 1 (Chapter 2.5), Pergamon Press, Oxford, 1991, p. 579 (Chapter 2.5).
[8] J.L. Speier, J.A. Webster, G.H. Barnes, J. Am. Chem. Soc. 79 (1957) 974.
[9] S. Thorimbert, G. Giambastiani, C. Commandeur, M. Vitale, G. Poli, M. Malacria, Eur. J. Org. Chem. (2003) 2702.
[10] C. Reichardt, Solvents and Solvents Effects in Organic Chemistry, second ed., VCH, Weinheim, 1988, p. 408.
[11] A.D. Becke, J. Chem. Phys. 98 (1993) 5648.
[12] C. Lee, W. Yang, R.G. Parr, Phys. Rev. B 37 (1988) 785.
[13] M.J. Frisch, G.W. Trucks, H.B. Schlegel, G.E. Scuseria, M.A. Robb, J.R. Cheeseman, V.G. Zakrzewski, J.A. Montgomery Jr., R.E. Stratmann, J.C. Burant, S. Dapprich, J.M. Millam, A.D. Daniels, K.N. Kudin, M.C. Strain, O. Farkas, J. Tomasi, V. Barone, M. Cossi, R. Cammi, B. Mennucci, C. Pomelli, C. Adamo, S. Clifford, J. Ochterski, G.A. Petersson, P.Y. Ayala, Q. Cui, K. Morokuma, D.K. Malick, A.D. Rabuck, K. Raghavachari, J.B. Foresman, J. Cioslowski, J.V. Ortiz, B.B. Stefanov, G. Liu, A. Liashenko, P. Piskorz, I. Komaromi, R. Gomperts, R.L. Martin, D.J. Fox, T. Keith, M.A. Al-Laham, C.Y. Peng, A. Nanayakkara, C. Gonzalez, M. Challacombe, P.M.W. Gill, B. Johnson, W. Chen, M.W. Wong, J.L. Andres, C. Gonzalez, M. Head-Gordon, E.S. Replogle, J.A. Pople, Gaussian 98, Revision A.5; Gaussian Inc., Pittsburgh, PA, 1998.
[14] P.J. Hay, W.R. Wadt, J. Chem. Phys. 82 (1985) 299.
[15] T.H. Dunning, Jr., P.J. Hay, in: H.F. Schaeffer, III (Ed.), Modern Theoretical Chemistry, vol. 3, Plenum, New York, 1976, p. 1.
[16] (a) W.J. Hehre, R.F. Stewart, J.A. Pople, J. Chem. Phys. 51 (1969) 2657;
(b) W.J. Hehre, R. Ditchfield, R.F. Stewart, J.A. Pople, J. Chem. Phys. 52 (1970) 2769.
[17] (a) A. Klamt, G. Schüürmann, J. Chem. Soc. Perkin Trans. 2 (1993) 799;
(b) V. Barone, M. Cossi, J. Phys. Chem. A 102 (1998) 1995.
[18] (a) T. Ziegler, A. Rauk, Theor. Chim. Acta 46 (1977) 1;
(b) T. Ziegler, A. Rauk, Inorg. Chem. 18 (1979) 1558.
[19] (a) ADF 1999, E.J. Baerends, A. Bérces, C. Bo, P.M. Boerrigter, L. Cavallo, L. Deng, R.M. Dickson, D.E. Ellis, L. Fan, T.H. Fischer, C. Fonseca Guerra, S.J.A. van Gisbergen, J.A. Groeneveld, O.V. Gritsenko, F.E. Harris, P. van den Hoek, H. Jacobsen, G. van Kessel, F. Kootstra, E. van Lenthe, V.P. Osinga, P.T.H. Philipsen, D. Post, C.C. Pye, W. Ravenek, P. Ros, P.R.T. Schipper, G. Schreckenbach, J.G. Snijders, M. Solà, D. Swerhone, G. te Velde, P. Vernooijs, L. Versluis, O. Visser, E. van Wezenbeek, G. Wiesenekker, S.K. Wolff, T.K. Woo, T. Ziegler, Scientific Computing & Modelling NV, Amsterdam, The Netherlands, 1999. Available from http://www.scm.com.;
(b) C. Fonseca Guerra, J.G. Snijders, G. te Velde, E.J. Baerends, Theor. Chem. Acc. 99 (1998) 391.
[20] A.D. Becke, Phys. Rev. A 38 (1988) 3098.
[21] E.J. Baerends, D.E. Ellis, P. Ros, Chem. Phys. Lett. 2 (1973) 41.